The effect of diffusion constrains and ZnO_x speciation on non-oxidative dehydrogenation of propane and isobutane over ZnO-containing catalysts

Dan Zhao[1,2 †], Mingbin Gao[3 †], Xinxin Tian[1,4 †], Dmitry E. Doronkin[5], Shanlei Han[1,2], Jan-Dierk Grunwaldt[5], Uwe Rodemerck[1], David Linke[1], Mao Ye[3], Guiyuan Jiang[2], Haijun Jiao[1], Evgenii V. Kondratenko[1*]

[1]*Leibniz-Institut für Katalyse e.V., Albert-Einstein-Strasse 29a, D-18059 Rostock, Germany*

[2]*State Key Laboratory of Heavy Oil Processing, China University of Petroleum, Beijing, Beijing, 102249, P. R. China*

[3]*National Engineering Laboratory for Methanol to Olefins, Dalian National Laboratory for Clean Energy, iChEM (Collaborative Innovation Center of Chemistry for Energy Materials), Dalian Institute of Chemical Physics, Chinese Academy of Sciences, Dalian 116023, P. R. China.*

[4]*Key Laboratory of Materials for Energy Conversion and Storage of Shanxi Province, Institute of Molecular Science, Shanxi University, Taiyuan 030006, P. R. China*

[5]*Institute of Catalysis Research and Technology and Institute for Chemical Technology and Polymer Chemistry, Karlsruhe Institute of Technology (KIT), Engesserstr.20, 76131 Karlsruhe, Germany*

† These authors contributed equally to this work.

*Correspondence to: evgenii.kondratenko@catalysis.de (E.V.K.)

Abstract

Heterogeneously catalyzed gas-solid-phase reactions are generally suffered from diffusion limitations in large-scale processes or in academic studies when zeolites were used as catalysts or supports. Here, we elucidated the effects of diffusion of reactants/products in non-oxidative propane (PDH) and isobutane dehydrogenation (iBDH) reactions on performance of catalysts based silicalite-1(S-1), dealuminated Beta (deAl Beta), and ZrO_2 and possessing differently structured ZnO_x species. The catalysts were prepared through physically mixing ZnO and the support. The force field molecular dynamics simulations revealed the effectiveness factor η larger than 0.8 in the PDH reaction over all catalysts thus suggesting that mass transport limitations do not play any significant role. However, the iBDH reaction over S-1-based catalysts suffers from severe diffusion limitations ($\eta<0.45$). Such conditions are favorable for cracking reactions responsible for isobutene selectivity loss. To compare intrinsic catalyst activity in the PDH and iBDH reactions over ZnO_x/S-1 catalyst, molecular-level insights into individual reaction pathways were derived from Density Functional Theory calculations.

The nature of active ZnO_x sites was investigated by X-ray absorption spectroscopy and was established to depend on the kind of support material. Binuclear ZnO_x species are formed inside small S-1 pores or on the surface of ZrO_2, while three-dimensional multinuclear ZnO_x clusters are generated in the Beta zeolite with larger pores. The latter show higher Zn-related activity in the PDH reaction under conditions free of any diffusion constrains. The developed ZnO-deAl Beta showed the space time yield of propene or

isobutene formation of 2 kg_{C3H6} $kgcat^{-1}$ h^{-1} or 6.3 $kg_{i\text{-}C4H8}$ $kgcat^{-1}$ h^{-1} at 550°C and about 65% equilibrium alkane conversion with olefin selectivity of about 90%. The activity values are higher than those reported for the state-of-the-art non-noble metal oxide catalysts tested at the same or even higher temperatures.

KEY WORDS: ZnO_x species; zeolite; diffusion constrains; non-oxidative dehydrogenation; propane; isobutane

1 INTRODUCTION

It is commonly accepted that heterogeneously catalyzed reactions (gas-solid phase) follow five general steps, i.e., (i) diffusion (from the bulk gas to the external catalyst surface or within catalyst pores) of reactants towards catalyst surface, (ii) their adsorption on active sites, (iii) chemical transformations, (iv) desorption of formed reaction products and finally (v) their diffusion (from the external catalyst surface or within catalyst pores to bulk gas,) towards the gas phase[1]. Therefore, the diffusion of reactants/products may play an important role in the gas-solid phase reactions, especially when porous materials are used as catalysts or supports. All academic studies, in principle, should be carried out under the conditions free of mass transport limitations as required for assessing intrinsic catalyst activity and selectivity. Many studies, however, did not consider the diffusion behaviors of reactants/products to the internal surface of porous materials where the active sites mainly locat[2-4]. In addition, such constrains are practically unavoidable under large-scale operation because of the size of catalyst particles or for highly active catalysts even under lab conditions. Thus, it is important to understand the consequences of such limitations for catalyst activity and particularly for selectivity to gas-phase products and to carbon-containing deposits in the high-temperature reactions [5-6].

The non-oxidative dehydrogenation (DH) of light alkanes, e.g., propane (PDH) or isobutane (iBDH), is one of the most promising on-purpose technologies to produce the corresponding alkenes[7-9] over Pt-[10-12] or Cr-based[13] catalysts. These catalysts, however,

suffer from high costs and necessity of using Cl-containing compounds[14] to re-disperse large Pt particles, or the toxic nature of Cr(VI) compounds. Encouraged by the requirements of environmental sustainability, many efforts have been made both in academia and industry to develop alternative supported or bulk DH catalysts based on oxides of V[15-16], Ga[17-18], Co[19], Fe[20-21] or Zr[22-23]. ZnO-containing catalysts based on metal oxides, e.g., SiO_2[24], Al_2O_3[25], ZrO_2-based materials[26-27], and zeolites, e.g., HZSM-5[28-29], dealuminated (deAl) Beta[30] and silicalite-1(S-1)[31-35] were widely investigated. However, based on the above-mentioned five general steps in the gas-solid reactions, the diffusion effect on the catalyst activity and product selectivity could not be ignored when zeolites are used as catalysts or supports.

Against the above background, our present intentions are to explore (i) the effect of the topology of support on catalyst activity and product selectivity and (ii) the efficiency of catalysts used in PDH and iBDH. To this end, S-1 (10 member-ring pores), deAl Beta zeolite (12 member-ring pores) as well as non-porous ZrO_2 were used as supports for well-defined ZnO_x species. The structure of ZnO_x species was determined by X-ray absorption spectroscopy. Sophisticated kinetic DH tests in a broad range of alkane conversion degrees and at different reaction temperatures enabled to elucidate fundamentals related to the formation of individual products. Molecular diffusion simulations provided the basis for establishing the relationship between catalyst structure, mass transport, and DH performance, i.e., activity and product selectivity. Knowing the structure of active ZnO_x

species in ZnO_x/S-1, Density Functional Theory (DFT) calculations were applied to reveal molecular-level pathways of propene or isobutene formation in PDH or iBDH.

2 EXPERIMENTAL SECTION

2.1 Catalyst Preparation

The preparation method of silicalite-1 (S-1(1)) has been reported in our previous work[35]. This zeolite was synthesized from the following gel composition in a molar ratio of 1 SiO_2: 0.175 TPAOH: 15.4 H_2O. Typically, 48.8 g of 25 wt% TPAOH (tetrapropylammonium hydroxide, Shanghai Cairui Chemical Engineering Technology Co. Ltd, 25 wt% water solution) were mixed with 25.9 g of deionized water and stirred at room temperature for 10 min. 50.0 g of TEOS (tetraethyl orthosilicate, Sinopharm Chemical Reagent Co. Ltd) were added to the above solution and the resulting mixture was aged at room temperature for additional 6 h. Afterwards, the transparent solution was transferred to a stainless-steel autoclave with a PTFE insert and heated to 100 ℃ for 48 h. After cooling down to room temperature, the solid material was separated from the mother liquid by centrifugation and re-dispersed in deionized water for washing. This process was repeated three times. After desiccation, the zeolite precursor was calcined in static air at 550 ˚C for 6 h.

S-1(2) and S-1(3) were synthesized from the gels with the following compositions (molar ratio): 1 SiO_2: 0.15 TPAOH: 15.4 H_2O: 0.5 g seed and 1 SiO_2: 0.15 TPAOH: 49.2 H_2O, respectively. TEOS or silica sol (40 wt% SiO_2) was used as the Si source for the preparation of S-1(2) or S-1(3). The crystallization temperature and time were 170 ℃ and 48 h for both

samples. After crystallization, the solid products were collected by filtration followed by washing, desiccation and calcination in static air at 550 ℃ for 6 h.

A beta zeolite (Si/Al_2=25) was purchased from Nankai University Catalyst Co. Ltd. To remove framework aluminum, 10 g of the zeolite were treated in 200 mL of concentrated HNO_3 at 120 ℃ for 10 h. The washed and then dried material was re-dispersed in diluted HNO_3 (200 mL, $V_{(HNO3)}$: $V_{(H2O)}$=3:1) and stirred at room temperature for 5 h to remove extra-framework Al species. Hereafter, the solid product was collected after filtration, washing, desiccation and abbreviated as deAl Beta. ZrO_2 was provided by Daiichi Kigenso Kagaku Kogyo Co. and was used without any treatment.

ZnO-based catalysts were synthesized as follows. 0.08 g of commercial ZnO (Sigma-Aldrich) and 0.92 g of each support were physically mixed in a mortar for 10 min. Afterwards, the mixtures were pressed and sieved to 315-710 μm. The as-prepared catalysts were abbreviated as ZnO-support. For example, ZnO-S-1(1) stands for the sample in which ZnO and S-1(1) were used.

For X-ray absorption spectroscopy (XAS) measurements (see section 2.2), to exclude the effect of bulk ZnO present in the above-described physical mixtures, additional catalysts were prepared according to a dual-bed method shown in Scheme 1. Typically, commercial ZnO (particles of 315-710 μm) and support (particles of 315-710 μm) were loaded into a quartz tube (inner diameter of 6 mm) with ZnO being the top layer (upstream). The ZnO (50 mg) and support layers (100 mg) were separated by a quartz wool layer (about

10 mg). The loaded reactors were initially heated to 550 ºC in Ar (10 mL min^{-1}) with a heating rate of 10 ºC·min^{-1} followed by exposure to a flow of air (10 mL min^{-1}) for 1 h at the same temperature. Hereafter, Ar was fed for 15 min to remove air from the reactors and then this flow was replaced by a flow of 50 vol% H_2 in Ar (10 mL min^{-1}) for 1 h. The reactors were afterward cooled down to room temperature in Ar. Finally, the bottom layer containing the support with deposited ZnO_x species was collected and used for XAS measurements. To distinguish from the physically mixed catalysts described above, the catalysts prepared according to Scheme 1 are named as ZnO_x/support. Zn loading in the prepared ZnO_x/S-1(1), ZnO_x/deAl Beta and ZnO_x/ZrO_2 are 1.20, 0.86 and 1.60 wt%, respectively.

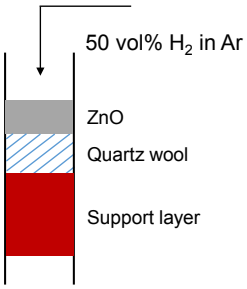

Scheme 1 A schematic illustration of reactor loading for preparation of ZnO_x/support catalysts used for XAS measurements.

2.2 Catalyst Characterization

To determine the surface area of different supports, N_2 adsorption-desorption measurements were carried out on ASAP 2020 (Micromeritics, USA). Before the tests, all samples were pretreated at 300 ℃ in N_2 for 3 h to remove physically adsorbed water. Afterwards, N_2 adsorption-desorption measurements were carried out at 77 K.

The topography and particle size of different supports were characterized by scanning electron microscopy (SEM) using a Sigma 500 (Zeiss) microspore operating at an accelerating voltage of 5 kV.

Acidic properties of zeolites were analyzed by temperature-programmed desorption measurements with NH_3 (NH_3-TPD) using an in-house developed setup containing 8 individually heated continuous-flow fixed-bed quartz reactors. Each catalyst (50 mg) was initially heated to 550 °C in a flow of Ar followed by feeding air for 1 h and then cooled down to 120 °C. Then, the catalysts were exposed to a flow of 1 vol% NH_3 in Ar for 1.5 h at the same temperature. To remove physically adsorbed NH_3, the catalysts were further flushed in Ar at 120 °C for 2 h and then cooled to 80 °C. Finally, the treated catalysts were individually heated to 900 °C with a heating rate of 10 °C·min^{-1}. NH_3 and Ar were detected at the reactor outlet by an on-line mass spectrometer at m/z of 15 and 40, respectively.

To explore the nature of active ZnO_x species, X-ray absorption near edge structure (XANES) and extended X-ray absorption fine structure (EXAFS) spectra at the Zn K absorption edge were recorded at the P65 beamline of the PETRA III synchrotron (DESY, Hamburg) in transmission mode except for the ZnO_x/ZrO_2 sample. It was analyzed in fluorescence mode using a silicon drift detector (Hitachi Vortex ME4). The energy of the X-ray photons was selected by a Si(111) double-crystal monochromator and the beam size was set by means of slits to 0.2(vertical) × 1.5(horizontal) mm^2. Using the ATHENA program from the IFEFFIT software package[36], the recorded spectra were normalized and

the EXAFS background was subtracted. The k^2-weighted EXAFS functions were Fourier transformed (FT) in the k range of 2.5-12.3 $Å^{-1}$. The amplitude reduction factor S_0^2=1.05 was obtained through fitting the reference spectrum of crystalline ZnO to a wurtzite structural model (Inorganic Crystal Structure Database, collection code is 34477). The Artemis[36] software was applied to fit the EXAFS data according to a least square method in the R-space between 1.0 and 3.2 Å. The model with two shells from the wurtzite structure (Zn-O and Zn-Zn) was used for the fits. To fit the second shell of the spectrum of ZnO_x/ZrO_2 sample with physically meaningful values, it was necessary to increase the starting interatomic distance for this shell by ca. 0.2 Å relative to the distance found in the original ZnO model. Interatomic distances (r), energy shift (δE_0), coordination numbers (CN) and mean square deviation of interatomic distances (σ^2) were refined during the fitting. The absolute misfit between the theory and the experiment is expressed by ρ.

2.3 Catalytic Tests

PDH or iBDH tests were carried out in an in-house developed setup equipped with 15 continuous-flow tubular fixed-bed quartz reactors. A feed containing either 40 vol% propane or 40 vol% isobutane in N_2 was used in all tests. To determine the rate of propene or isobutene formation, the degree of propane or isobutane conversion was below 10%. The samples were initially heated to 550 ℃ in N_2 (15 mL·min^{-1}), and then flushed in a flow (10 mL·min^{-1}) of air at the same temperature for 1 h. After 15 min purging in N_2 (10 mL min^{-1}), the catalysts were exposed to a flow (10 mL·min^{-1}) of 50 vol% H_2 in N_2 for 1 h followed by flushing with N_2 (10 mL·min^{-1}) for 15 min and finally feeding either propane

or isobutane (40 vol% C_3H_8 or iso-C_4H_{10} in N_2). The rates of propene or isobutene formation were calculated according to eq. 1.

$$r(C_nH_{2n}) = \frac{\dot{n}(C_nH_{2n})}{m(cat)} \quad \text{eq.1}$$

where $\dot{n}(C_nH_{2n})$ and m(cat) stand for the molar flow of propene or isobutene (mmol min^{-1}) and catalyst mass (g), respectively.

Long-term stability PDH or iBDH tests were carried out at 550 ℃ with a feed of C_nH_{2n+2}:N_2=2:3 (n=3 or 4). The catalyst treatment was same as for determining the initial activity of reduced catalysts. The degrees of propane conversion and isobutane conversion were adjusted to about 30 and 45% by varying contact time. The conversion of alkanes, the selectivity to gas-phase products and coke were determined according to eqs. 2-4, respectively. Equation 5 was used to calculate the space time yield (STY) of propene or isobutene formation.

$$X(C^nH^{2n+2}) = \frac{\dot{n}^{in}_{C_nH_{2n+2}} - \dot{n}^{out}_{C_nH_{2n+2}}}{\dot{n}^{in}_{C_nH_{2n+2}}} \quad \text{eq. 2}$$

$$S(i) = \frac{\beta_i \quad \dot{n}_i^{out}}{\beta_{C_nH_{2n+2}}\dot{n}^{in}_{C_nH_{2n+2}} - \dot{n}^{out}_{C_nH_{2n+2}}} \quad \text{eq. 3}$$

$$S(coke) = 1 - \sum_i S(i) \quad \text{eq. 4}$$

$$STY = \frac{\dot{n}_{C_nH_{2n}} \times M_{C_nH_{2n}} \times 60}{1000 \times m_{cat}} \quad \text{eq. 5}$$

where ṅ with superscripts “in” or “out” means the molar flow of gas-phase components at the reactor inlet or outlet (mmol·min^{-1}). βi represents the stoichiometric coefficient for the product i. $M_{C_nH_{2n}}$ is the molecular weight of propene or isobutene (42 g·mol^{-1} or 56 g·mol^{-1}).

The rate constant of catalyst deactivation was calculated from the long-term stability tests according to eq. 6 as suggested in Ref.[37].

$$k_{deactivation} = \frac{\ln\left(\frac{1 - X(C_nH_{2n+2})_{final}}{X(C_nH_{2n+2})_{final}}\right) - \ln\left(\frac{1 - X(C_nH_{2n+2})_{initial}}{X(C_nH_{2n+2})_{initial}}\right)}{t} \quad \text{eq. 6}$$

Turnover frequency (TOF) values were calculated in two different ways. Either the total amount of Zn or the geometric structure of ZnO_x species were considered as shown in eq. 7-8,

$$TOF\_total = \frac{r(C_3H_6) \times 60}{n_{total\ Zn}} \quad \text{eq. 7}$$

$$TOF\_geo = \frac{r(C_3H_6) \times 60 \times (CN + 1)}{n_{total\ Zn}} \quad \text{eq. 8}$$

where $r(C_3H_6)$ is the rate of propene formation calculated by eq.1, CN is the coordination number of Zn-Zn determined by EXAFS.

To determine an apparent activation energy of propene or isobutene formation, the corresponding rates were determined at 475, 500, 525 and 550 ℃. The energy values were obtained from the slope of the dependence of $\ln(r(C_3H_6))$ or $\ln(r(iso\text{-}C_4H_{10}))$ versus 1/T. Prior to the tests, the catalysts were initially reduced at 550 ºC in 50 vol% H_2 in N_2 for 1 h, and then cooled down to a target temperature.

An on-line gas chromatograph (GC, Agilent 6890) equipped with flame ionization (FID) and thermal conductivity (TCD) detectors was used to analyze and quantify the feed components and the reaction products. The GC has PLOT/Q (for CO_2), AL/S (for hydrocarbons), and Molsieve 5 (for H_2, O_2, N_2, and CO) columns. The GC analysis time of gas-phase components is 4 minutes and 9 minutes for PDH and iBDH, respectively.

2.4 Molecular Diffusion Simulations

2.4.1 Force Field Molecular Dynamics Simulation

Force field molecular dynamics (FFMD) simulation is an effective approach to analyze the diffusivity of guest molecules within zeolite framework[38-40]. All molecular dynamics (MD) simulations were carried out using the Materials Studio simulation package (Accelrys Software). Adsorption/desorption behavior of propane/propene or isobutane/isobutene in the BEA and MFI frameworks was calculated using the grand canonical Monte Carlo (GCMC) simulation method. Periodic boundary conditions were applied in all three directions. The interatomic interactions were described by the condensed-phase-optimized molecular potentials for atomistic simulation studies (COMPASS) force field. The electrostatic energy was calculated by the Ewald & Group summation method. The Ewald & Group summation method has an Ewald accuracy of $4.18 \cdot 10^{-5}$ kJ·mol^{-1} for calculating the electrostatic potential energy. To achieve an equilibrium state, 10^7 Monte Carlo steps were carried out. The zeolitic framework with a rigid structure was considered. The metropolis scheme was used at a constant loading and constant temperature. To minimize the energy of constructed structures, all the structures were equilibrated by five annealing cycles from -73 ^{o}C to 627 ^{o}C with a heating ramp of 5 ^{o}C/min to refine the conformation. Dynamic processes in the NVT ensemble, where the number of particles (N), volume (V) and temperature (T) were kept as constants, were performed for 5000 ps in 5000000 steps after the systems have been equilibrated at 60 ^{o}C

and 550 °C. The velocity Verlet algorithm was used to integrate the Newton's equations of motion with a time step of 1 fs. A cutoff radius of 18.5 Å was assumed for Lennard-Jones interaction potential calculation. The simulated temperature was controlled by a Nosé thermostat. The structures considered in this study are shown in Figure S1. The slope of mean square displacement (MSD) as a function of time was used to determine the self-diffusivity following the Einstein relation (eq. 7).

$$MSD(\tau) = 2nD\tau + b \qquad \text{eq. 7}$$

where τ is the diffusion time, D is the intracrystalline diffusivity, n is the dimension of framework (n = 1, 2 and 3 for 1D, 2D and 3D frameworks, respectively) and b is the thermal factor arising from atomic vibrations.

2.4.2 Ab initio Molecular Dynamics Simulations

To consider the flexibility of zeolite framework, ab initio molecular dynamics (AIMD) simulations were applied, although at higher computational cost[41-42]. They were carried out with the CP2K simulation package (version 7.1)[43] with a GPW (Gaussian and plane wave) basis set[44]. At a theoretical level, the *rev*PBE functional was chosen due to its higher preciseness for the solid-state calculations in comparison with PBE functional. The *rev*PBE-D3 functional[45] with a plane wave cut-off at a density functional theory level combined with a DZVP (double-zeta valence polarized) basis set and GTH (Goedecker–Teter–Hutter) pseudopotentials[46] was applied. The cut-off energy was set to 350 Ry. A 1×1×1 supercell is employed for both BEA and MFI zeolite for the first principal simulations. Dispersion interactions are incorporated by means of the D3 corrections of

Grimme et al.[47-48] For each guest molecule, cell parameters were obtained by computing time-averaged values from a 10 ps *NpT* (amount *N*, pressure *p* and temperature *T*) molecular dynamics simulation at 550 °C and ambient pressure. Production molecular dynamics, which were used as input for the mobility analysis, were carried out in the NVT (amount N, volume V and temperature T) ensemble at 550 °C for 50 ps. The temperature of the simulations was controlled with a Nosé-Hoover chain thermostat[49-50] consisting of three beads and with a time constant of 1000 wavenumbers. The pressure was controlled with a Martyna-Tobias-Klein barostat[51-52]. A time step of 0.5 fs is employed for integrating the equations of motion[41]. The self-consistent field convergence criterion was set at 10^{-6}.

2.5 Density Functional Theory Calculations

Using the model for a binuclear ZnO_x species in ZnO_x/S-1 from our previous PDH study[32], elementary pathways in the course of iBDH were theoretically determined. Spin-polarized and periodic Density Functional Theory (DFT) calculations were carried out with the Vienna ab initio simulation package (VASP)[53-54]. The generalized gradient approximation in the Perdew-Burke-Ernzerhof (GGA-PBE) functional[55-56] was used to treat the electron exchange and correlation energies. The cut off energy was set up to 400 eV. Geometry optimization was converged until forces acting on atoms were lower than 0.02 eV/Å, and the energy difference was lower than 10−4 eV. The Climbing Image Nudged Elastic Band (CI-NEB) method was applied for identifying transition states[57]. All our reported energies include dispersion (D3)[49] and ZPE corrections (PBE+D3+ZPE).

3 RESULTS AND DISCUSSION

3.1 Physicochemical Properties of Supports and Reactants

As catalytically active ZnO_x species are located in the micropores of zeolite supports[32], propane or isobutane diffusion to the active sites can be essential in the PDH or iBDH reactions. Therefore, we firstly consider the topology of supports and the molecular size of the feed alkanes. The MFI zeolite possesses straight and sinusoidal channels with 10-member rings (Figure 1a). The pore sizes are 5.3 × 5.6 Å and 5.1 × 5.5 Å, respectively. The BEA zeolite has 3-dimensional intersecting 12-member rings (Figure 1b), which are larger than those in the MFI zeolite. Propane with the molecular size of 4.3 Å (Figure 1c) can enter the channels of both zeolites easier in comparison with isobutane having the molecular size of 5.3 Å (Figure 1d). Moreover, according to the simulation results in Ref.[58], isobutane was considered as a spherical molecule and its project diameter is as large as 7.0 Å, which is close to the pore size of the BEA zeolite along [100]. Therefore, the diffusion effect of reactants within the zeolites should be considered, especially in the iBDH reaction. To mimic their diffusion, force field molecular dynamics (FFMD) simulation was employed at the reaction temperature (see **Theoretical Analysis of Diffusivity of Propane and Isobutane** section).

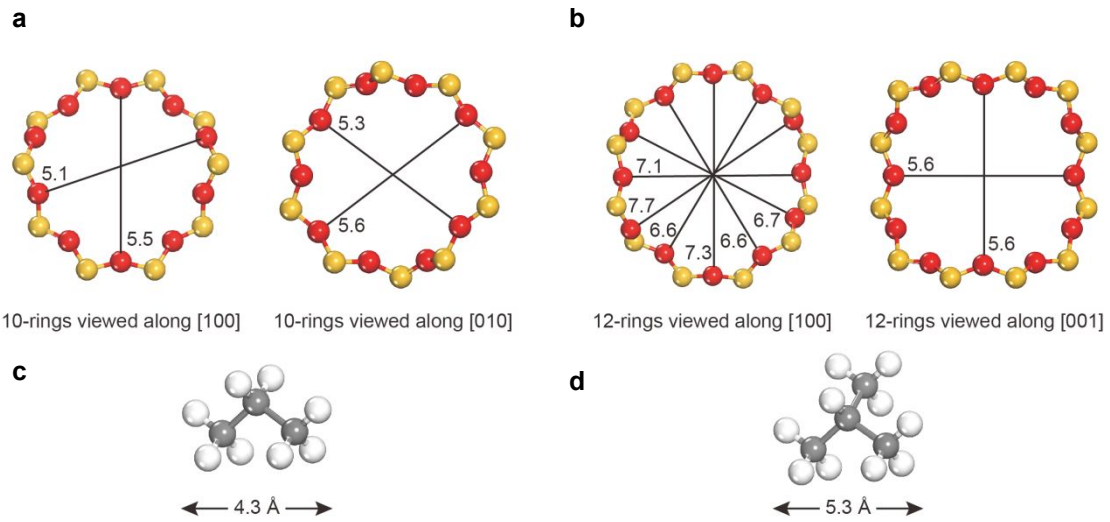

Figure 1 The topology of (a) MFI and (b) BEA zeolites, the dynamic diameters of (c) propane and (d) isobutane. Yellow, red, grey and white stand for Si, O, C and H atom, respectively.

The morphology of different zeolites was also investigated by SEM (Figure S2). Among different S-1 supports, the S-1(1) possesses spherical particles with the smallest particle size of ~80 nm (Figure S2a). Consequently, this material has the highest external surface of 86 m^2 g^{-1} and the volume of mesopores of 0.49 cm^3 g^{-1} (Table 1). The particle sizes of S-1(2) and S-1(3) are larger than that of S-1(1), with about 200 nm and 8 μm (Figure S2b and c), respectively. The morphology of deAl Beta zeolite is different from that of the S-1 samples and the particle size distribution is not uniform (Figure S2d). Due to the larger pore size and lower density of framework, deAl Beta processes the highest surface area among all zeolitic supports in the present study. ZrO_2 does not possess any microporous structures and has the lowest surface area of 108 m^2 g^{-1}.

Table1 The specific (S_{BET}) and external ($S_{external}$) surface areas, the surface area of micropores (S_{micro}) as well as volumes of micro- (V_{micro}) and mesopores (V_{meso}) of different supports.

Supports	S_{BET} / $m^2\ g^{-1}$	$S_{external}$/[a] $m^2\ g^{-1}$	S_{micro} /[a] $m^2\ g^{-1}$	V_{micro} /[b] $cm^3\ g^{-1}$	V_{meso} /[b] $cm^3\ g^{-1}$
S-1(1)	462	86	376	0.17	0.49
S-1(2)	452	23	429	0.20	0.11
S-1(3)	406	23	383	0.19	0.07
deAl Beta	546	94	452	0.19	0.19
ZrO_2	108	-	-	-	0.31

[a] the $S_{external}$ and $S_{micropore}$ were obtained by t-plot method.

[b] the $V_{micropore}$ and $V_{mesopore}$ were obtained by BJH method.

3.2 Nature of Active ZnO_x Sites

An insight into the nature of active sites in ZnO_x-based catalysts were derived from XAS measurements. To avoid any effect from the bulk ZnO in the ZnO-zeolite mixtures, additional catalysts were prepared according to the dual-bed reduction method using H_2 as a reducing agent (Scheme 1 and the corresponding description in the experimental section). The position of the adsorption edge in the obtained XANES spectra of all as-prepared samples is about 9662 eV (Figure 2a), which is close to that of ZnO. Thus, the oxidation state of Zn in ZnO_x/S-1(1), ZnO_x/deAl Beta and ZnO_x/ZrO_2 is likely to be +2. The Fourier transformed k^2-weighted extended X-ray adsorption fine structure (EXAFS) spectra are presented in Figure 2b. The fitting results are summarized in Table 2 and Figure S3 in the Supporting Information. The first and second shell scatterings at 1.5 and 2.9 Å (3.2 Å for ZnO_x/ZrO_2 sample, uncorrected distance) correspond to O and Zn neighbors as in ZnO, respectively.

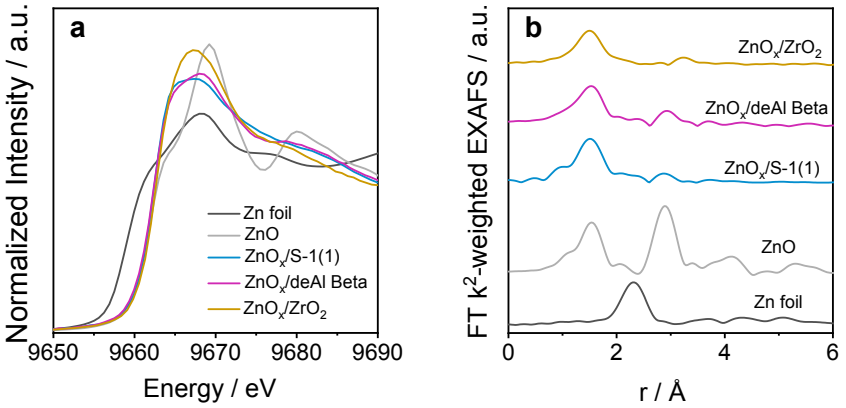

Figure 2 XANES spectra (a) and FT EXAFS spectra (b) (not corrected for the phase shift) of as-prepared samples and reference materials.

The average coordination number (CN) of Zn-Zn and Zn-O in ZnO_x/S-1(1) is 1 and 3, indicating that ZnO_x species exist in the form of binuclear ZnO_x species. In comparison with ZnO_x/S-1(1), the second shell of Zn-O in ZnO_x/deAl Beta is more pronounced. Considering the higher average CN of Zn-Zn in this species (Table 2), small 3-dimensional ZnO_x clusters should be formed in this catalyst. The distance of Zn-Zn in ZnO_x/ZrO_2 is about 0.2 Å longer than that in ZnO_x/S-1(1) and ZnO_x/deAl Beta catalyst (3.52 Å vs. 3.32 Å), and an extra Zn-O shell at a longer distance was needed for a better fit (lower ρ value). The CN number of Zn-Zn, however, is similar to that in ZnO_x/S-1(1) catalyst. Therefore, we put forward that binuclear ZnO_x species were also formed on the surface of ZrO_2 but with a different geometry.

Table 2 EXAFS fitting results

Catalyst	shell	CN	distance / Å	σ^2 / 10^{-3} Å^2	δE_0 / eV	ρ / %
ZnO_x/S-1(1)[a]	Zn-O	2.9±0.2	1.97±0.01	7.3±1.6	4.7±0.6	0.2
	Zn-Zn	1.3±0.5	3.32±0.07	7.3±1.6		
ZnOx/deAl Beta	Zn-O	2.9±0.1	1.98±0.01	7.3*	3.9±0.6	0.3
	Zn-Zn	6.1±2.1	3.30±0.02	18.7±4.1		
ZnO_x/ZrO_2	Zn-O	2.9±0.1	2.00±0.04	7.3*	-0.84±1.2	2.0
	Zn-Zn	1.1±0.5	3.52±0.03	7.3*		
	Zn-O	1.2±0.4	3.24±0.02	7.3*		

a The fitting data were taken from our previous study[32].

*Fixed at the most common value for room temperature measurements for the ease of data comparison.

3.3 Catalyst Activity in PDH and iBDH

ZnO-support (S-1(i), deAl Beta or ZrO_2) physical mixtures were initially tested at 550 ˚C in the PDH and iBHD reactions at degrees of alkane conversion below 10% to determine the rate of olefine formation. The catalysts were initially treated in a flow of 50 vol% H_2 in N_2 at the same temperature for 1 h. Such treatment is required to reduce ZnO to metallic Zn, which react with OH nests to form catalytically active ZnO_x species as demonstrated in our previous study[32]. Considering this information, the different activity of ZnO-S-1(i) mixtures both in the PDH and iBDH reactions (Figure 3a) can be explained by the different concentrations of OH nests in these support materials, i.e., 0.374, 0.960 and 0.265 mmol g^{-1} for S-1(1), S-1(2) and S-1(3), respectively (Figure S4). Such values were determined through a combination of in situ diffuse reflectance infrared spectroscopic (in situ DRIFTs) tests with temperature-programmed release of water measurements (Figure S4 a,b). The details were reported in our previous study[32]. Except for the deAl Beta support, a positively

linear correlation between the activity and the amount of OH nests on S-1 supports was established (Figure S4 c,d). This result is in line with the XAS results that different ZnOx clusters were formed on the deAl Beta support in comparison with S-1(1) support.

In PDH reaction, the highest rate of propene formation ($r(C_3H_6)$) was achieved over ZnO-S-1(2) and ZnO-deAl Beta (1.97 vs. 1.99 $mmol \cdot g^{-1} \cdot min^{-1}$). ZnO-$ZrO_2$ showed the second lowest $r(C_3H_6)$ of 0.78 $mmol \cdot g^{-1} \cdot min^{-1}$ (Figure 3a). When isobutane was dehydrogenated over the same catalysts, all of them showed higher activity in comparison with the PDH reaction. The strength of the increase in the rate of olefine formation, however, depends strongly on the support applied. In agreement with the PDH reaction, ZnO-deAl Beta is also the most active catalyst in the iBDH reaction. The rate of isobutene formation is 8.0 $mmol\ g^{-1}\ min^{-1}$ (Figure 3a). This rate over ZnO-S-1(2) is about 2 times lower although this catalyst performed very similarly as ZnO-deAl Beta in the PDH reaction (Figure 3a). To illustrate how the catalysts change their activity upon replacing propane by isobutane, we calculated the ratio of $r(iso\text{-}C_4H_8)/r(C_3H_6)$ that is shown in Figure 3b. This ratio is between 2 and 2.5 for the ZnO-S-1(i) catalysts but it is as high as 4 for the ZnO-deAl Beta and ZnO-ZrO_2 catalysts. In comparison with S-1(i), the supports in the latter two catalysts have larger pore size and open structure.

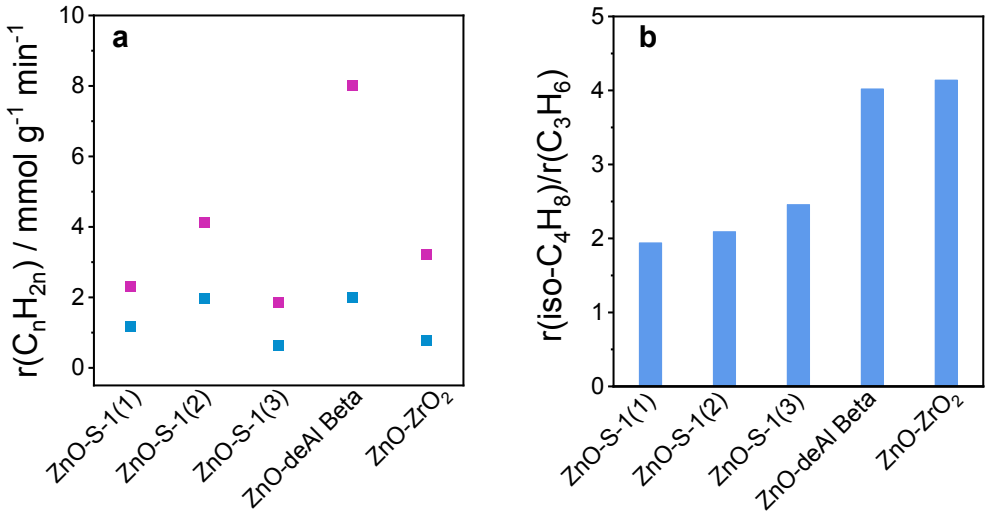

Figure 3 (a) The rate of propene (■) and isobutene (■) formation; (b) the ratio of r(iso-C_4H_8) and r(C_3H_6) over ZnO-support catalysts. Reaction conditions: 550 ℃, C_nH_{2n+2}:N_2=2:3, the total flow rate are 40 and 60 mL min^{-1} for the PDH and iBDH reactions.

We also determined an apparent activation energy (E_a) of olefin formation in the PDH and iBDH reactions in the temperature range from 475 to 550 ˚C. On this basis, the catalysts can be divided into three groups: ZnO-S-1(i), ZnO-deAl Beta and ZnO-ZrO_2. In the PDH reaction, the first group of catalysts is characterized by the E_a value of 99±3 kJ mol^{-1}, indicating that they have the same structure of active sites (Figure S5). A slightly higher value of 116 kJ mol^{-1} was determined for the ZnO-deAl Beta catalyst. The lowest activation energy of 86 kJ mol^{-1} was determined for ZnO-ZrO_2. This value is much lower than that for bare ZrO_2 (183 kJ mol^{-1}), where the active sites consisting of two coordinatively unsaturated Zr^{4+} sites are responsible for propane dehydrogenation as shown in our previous studies[22-23]. Considering the huge difference in the E_a values for ZrO_2 and ZnO-ZrO_2, the in situ formed ZnO_x species on the surface of ZrO_2 should catalyze the DH reaction rather than Zr^{4+} sites.

As expected from the lower C–H bond strength in isobutane than in propane, the E_a value of isobutene formation over ZnO-ZrO_2 or ZnO-deAl Beta is lower than that of propene formation, i.e., 51 vs 86 kJ mol^{-1} or 101 vs 116 kJ mol^{-1}. Contrarily, the E_a value of isobutene formation over ZnO-S-1(i) catalysts is 13-30 kJ mol^{-1} higher than that of propene formation in the PDH reaction. Considering the distinctive behavior of catalysts based on 10-member rings (ZnO-S-1(i)) or 12-member rings (ZnO-deAl Beta) or even non-porous supports (ZrO_2), we put forward that internal diffusion constrains can play an important role in the studied reactions (see section **Theoretical Analysis of Diffusivity of Propane and Isobutane**).

To compare the catalysts based on MFI and BEA zeolites as well as ZrO_2 and possessing different ZnO_x species in terms of their intrinsic activity, we calculated the TOF values of propene formation in two different ways (eqs. 7 and 8). As the iBDH reaction over ZnO-S-1(i) suffers from diffusion limitations, we did not compare the catalysts in this reaction. When using the total number of Zn atoms in the catalysts, the obtained TOF values for ZnO_x/S-1(1), ZnO_x/deAl Beta and ZnO_x/ZrO_2 are 239 h^{-1}, 272 h^{-1} and 227 h^{-1}, respectively. If we consider the real structure or geometry of ZnO_x species, the TOF values of the binuclear ZnO_x species in ZnO_x/S-1(1) and ZnO_x/ZrO_2 will be 478 h^{-1} and 454 h^{-1}, respectively. Such value for 3D ZnO_x clusters with a coordination number of Zn-Zn of 6.1±2.1 in ZnO_x/deAl Beta is, however, in the range of 1360-2448 h^{-1}. Regardless of the calculation method, the TOF value of sub-nanometer 3D ZnO_x cluster is higher than that

of binuclear ZnO_x species. Considering the lower reactivity of single Zn^{2+} sites on the surface of SiO_2[24] (0.77 h^{-1}) and in silicalite-1[31] (39.6 h^{-1}), we can conclude that the degree of oligomerization of ZnO_x species is an activity-governing descriptor if the ZnO_x clusters are sub-nanometer range.

3.4 Catalyst Industrial Relevance

Long-term catalyst stability and olefin productivity at industrially relevant degrees of alkane conversion over ZnO-zeolite samples were additionally tested. The degrees of propane and isobutane conversion was controlled at the range of 25-30% or 40-50%, respectively. In the PDH reaction, the least intrinsically active ZnO-S-1(1) and ZnO-S-1(3) catalysts show propene selectivity between 93 and 95% at comparable degrees of propane conversion (Figure S6 a,b). The selectivity to coke is about 5% (Figure S6 c). The selectivity to propene over the most active ZnO-S-1(2) and ZnO-deAl Beta catalysts is slightly below 90% during the first 0.5 h on propane stream and reaches about 93% at the end of test, while the selectivity to coke follows an opposite trend (Figure S6 b,c). The selectivity changes might be partially caused by a decrease in the conversion of propane. When isobutane was used instead of propane, the trends of conversion and product selectivity with rising reaction time are similar as in the PDH reaction (Figure S6e-f). The highest selectivity to isobutene between 85 and 87% at isobutane conversion degrees between 50 and 43%, respectively, was achieved over ZnO-deAl Beta. The selectivity to coke over this catalyst is about 5% only (Figure S6j). In additional, this catalyst also shows higher S(iso-C_4H_8) in comparison to ZnO-S-1(1) catalysts but similar S(coke).

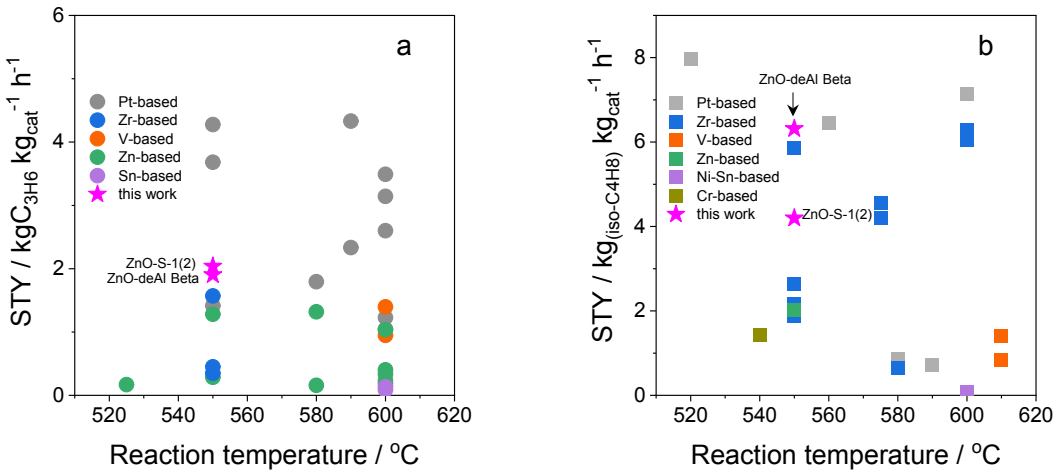

Figure 4 A comparison of the state-of-the-art catalysts and ZnO-based catalysts in PDH (a) and iBHD (b) reactions. The detailed data are available in Teble S1-2 in the supporting information.

To benchmark the most active ZnO-S-1(2) and ZnO-deAl Beta catalysts in terms of productivity, the initial space-time yield (STY) of propene or isobutene formation was calculated and is shown in

Figure 4a,b and Figure S6 d, h. The developed catalysts reveal higher STY(C_3H_6) and STY(iso-C_4H_8) values than the state-of-the-art non-noble metal oxide catalysts tested at the same or even higher temperatures (Table S1-2 and Figure 4).

Regardless of the reactants, all catalysts lose their initial activity (Figure S6 a, d) with rising time on alkane stream but with different rates (Table 3). The ZnO-deAl Beta shows the highest deactivation rate of 0.215 h^{-1} in the PDH reaction, which is about two times higher than that of ZnO-S-1(1). This is due to the higher selectivity to coke (Figure S6c). In the iBDH reaction, however, the deactivation rates of the most active three catalysts, i.e., ZnO-deAl Beta, ZnO-S-1(2) and ZnO-S-1(1), are comparable (0.117 vs. 0.120 vs. 0.123 h^{-1}). According to our previous studies[31-32, 35], the deactivation of ZnO-based

catalysts is mainly caused by (i) coke formation during DH reaction and (ii) irreversible Zn loss to a minor extent within 3 h on alkane stream. The prepared catalysts contain excessive ZnO (8 wt% ZnO), which could be transferred into catalytically active sites under reaction conditions and compensate their thermally induced loss. Thus, coke deposition on the catalyst surface should be the main reason for deactivation.

Table 3 The initial (after 4 or 9 minutes) and final (after 3 h) conversions of propane ($X(C_3H_8)$) and isobutane ($X(iso\text{-}C_4H_{10})$) as well as the deactivation rate constant (k_d) over different catalysts.

Catalyst name	$X(C_3H_8)$ / -		k_d in PDH	$X(iso\text{-}C_4H_{10})$ / -		k_d in iBDH
	initial	final	/ h^{-1}	initial	final	/ h^{-1}
ZnO-S-1(1)	0.26	0.21	0.101	0.47	0.38	0.123
ZnO-S-1(2)	0.31	0.24	0.118	0.46	0.38	0.120
ZnO-S-1(3)	0.23	0.20	0.065	0.41	0.38	0.035
ZnO-deAl Beta	0.30	0.18	0.215	0.51	0.42	0.117

3.5 Molecular-level Pathways in PDH and iBDH over Binuclear ZnO_x Species

To provide direct intrinsic kinetic insights into the PDH and iBDH reactions, we performed DFT calculations using a binuclear ZnO_x model (Figure S7), which was developed for PDH over ZnO_x/S-1 from Ref.[32]. Like propane, isobutane also has two activation pathways, i.e., (i) terminal methyl (CH_3) activation to get an isobutyl (i-butyl) intermediate and (ii) internal methine (CH) activation to get a tert-butyl (tert-butyl) intermediate. For the terminal CH_3 activation, there are two possible routes on the basis of surface structures (Figures S8-10, Table S3). The most favorable route is to form i-butyl

and hydroxyl intermediates (i-TS1 in Figure 5) with a barrier of 1.87 eV (endothermic by 0.51 eV). This barrier is higher than 1.35 eV required for cleavage of methylene C-H bond in propane. The formation of isobutene through H abstraction from the i-butyl intermediate also needs slightly higher energy than the formation of propene from the primarily formed i-propyl intermediate, i.e., 1.34 eV vs. 1.22 eV (i-TS2 and n-TS2 in Figure 5). The higher barriers for breaking both C-H binds in isobutane than in propane are associated with the larger size of isobutane and surface isobutyl as compared with propane and surface propyl (Figure S11). The final step in the PDH and iBDH reactions is the formation of H_2 from surface hydroxyl and a Zn-H-Zn intermediate and requires 1.07 eV in both reactions. Although it is easier to break C-H bonds in propane than in isobutane, the apparent barrier of the PDH reaction is higher than that of the iBDH reaction (1.87 eV vs. 1.59 eV in Figure 5). Nevertheless, the highest point on the potential energy surface for propane and isobutane is the re-combinative formation and desorption of H_2. Thus, in agreement with the experimental results (Figure 3), the rate of isobutene formation should be higher than the rate of propene formation.

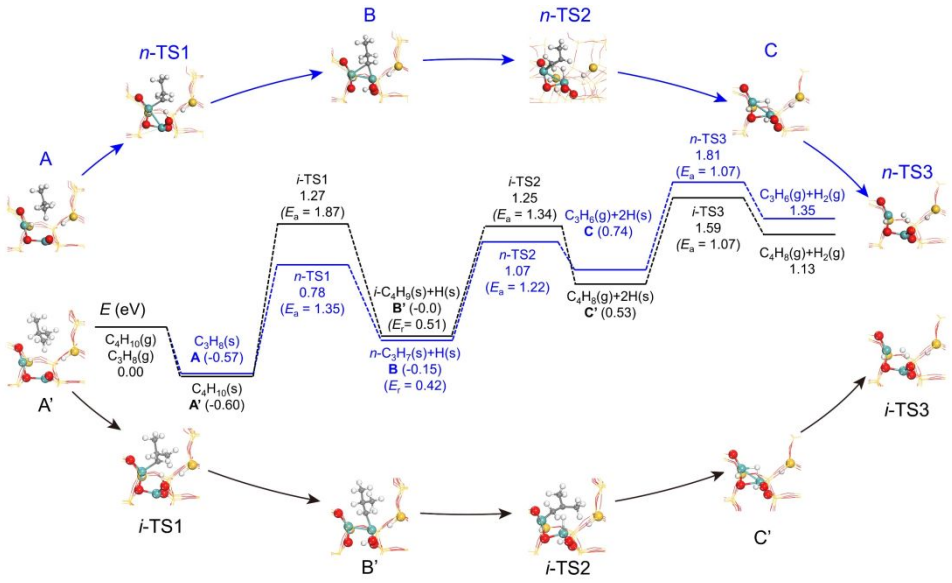

Figure 5 The potential energy surface of propane/isobutane dehydrogenation over a binuclear ZnO_x on the surface of S-1 from Ref.[32] at the PBE+D3+ZPE level.

3.6 Theoretical Analysis of Diffusivity of Propane and Isobutane

To investigate the shape selectivity of reactants imposed by zeolite topology from the perspective of molecular diffusion, FFMD simulations were applied according to previous studies[39-40, 59]. We initially validated our approach by comparing simulated and experimental diffusivity values. The simulated diffusion coefficients of propane and isobutane within the MFI framework at 60 °C agree well with those determined experimentally in Refs.[60-61] at the same temperature (Table S4, Figure S12a). Thus, our simulations at 550 °C (Figure S12 b, c) should also be reliable.

The FFMD simulations at 550 °C reveal a significant anisotropy phenomenon in the diffusion propane and isobutane within the BEA and MFI frameworks. The diffusivity (D_{yy}) along straight channel is 1.5-3 times higher than the diffusivity (D_{xx}) along sinusoidal channel (Figure 6a). Thus, the preponderant diffusion paths of propane and isobutane are

in sinusoidal channels. The difference in the molecular diffusion between propane and isobutane in the gas phase or within the zeolite framework is reflected by the ratio of $D_{C_3H_8}/D_{i^{so}\text{-}C_4H_{10}}$. Based on the kinetic gas theory of dilute gas[62], the diffusivities in the gas phase (D^{gas}) of propane and isobutane at 550 °C are 9.90×10^{-8} and 8.63×10^{-8} m^2 s^{-1}. Thus, the $D_{C_3H_8}/D_{i^{so}\text{-}C_4H_{10}}$ ratio should be close to 1.15 for the diffusion of these alkanes in the gas phase. The corresponding value calculated for their diffusion within the MFI and BEA frameworks is 18.69 and 1.28, respectively (Figure 6a, dark yellow circles). This implies that diffusion limitations within the MFI framework (10-member rings) are more severe than that within the BEA framework (12-member rings). Thus, the diffusion behavior of isobutane within the pore structure of ZnO-S-1(i) catalysts may have a crucial effect on catalyst performance in the iBDH reaction but not in the PDH reaction.

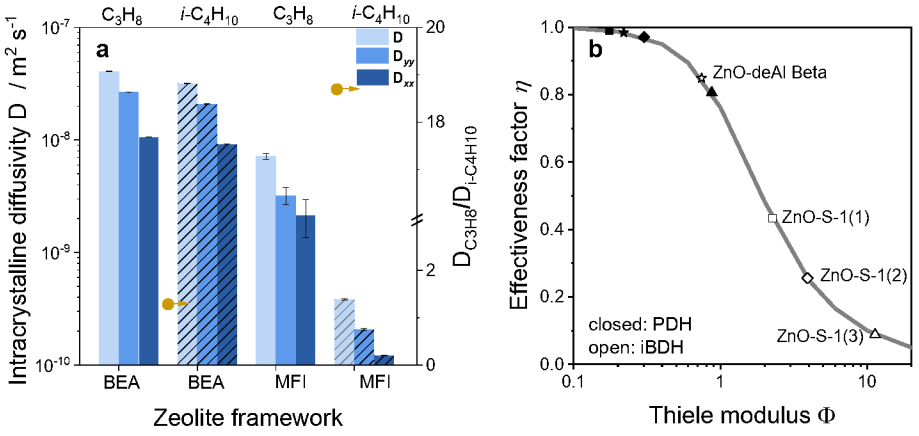

Figure 6 (a) The overall diffusivity D, diffusivity along straight channel D_{yy} and diffusivity along sinusoidal channel D_{xx} of propane and isobutane within the BEA and MFI zeolite frameworks and the ratio of $D_{propane}/D_{iso\text{-}butane}$ at 550 °C obtained by FFMD (dark yellow circles); (b) the effectiveness factor of PDH and iBDH over different catalysts used in this work.

Considering the less pronounced diffusion constrains of propane and isobutane at 550 °C within the BEA framework (Figure 6a), the rates of olefins formation in the PDH and iBDH reaction over ZnO-deAl Beta were used to represent the intrinsic reaction rates. The effectiveness factor η for the PDH and iBDH reactions was calculated according to $\eta = \tanh\phi/\phi$ using the Thiele modulus Φ analysis method and represents the effect of diffusion constrains on the utilization efficiency of these catalysts. Thiele modulus Φ is defined as $\phi = l\sqrt{k/D}$, where *l* is the distance from the center to the surface of zeolite along the straight channel, *k* is the reaction rate constant (these values for PDH and iBDH were obtained according to the experimental results based on the ZnO-delAl beta catalyst). The reaction rate constant is calculated by k = Aexp(-Ea/RT), where A is the pre-exponential factor, which is assumed to be 10^{13} s^{-1}[63]. The E_a values of PDH and iBDH on ZnO-delAl Beta catalyst are 116 and 101 kJ mol^{-1}. *D* is the intracrystalline diffusivity of a guest molecule. According to the analysis, all catalysts used for the PDH reaction are in the full-use regime (η>0.8) without any significant effect of mass transport (Figure 6b). This is also valid for the iBDH reaction over the ZnO-deAl Beta catalyst, while all the ZnO-S-1(i) catalysts have poor utilization efficiency (η<0.45) in this reaction. They can be ordered with this regard as follows: ZnO-S-1(1)>S-1(2)>S-1(3). This order correlates with the particle size of support in b axis; the larger the size is, the lower the efficiency is.

To consider the flexibility of zeolite framework, *ab initio* molecular dynamics (AIMD) simulations were applied[41-42]. The relative position between centroid of iso-butane and selected oxygen atom in BEA and MFI frameworks were determined at 550 °C by AIMD

(Figure 7a, b). The relative displacement of iso-butane within BEA framework during simulation period (50 ns) is significantly higher than that within MFI framework (Figure 7c). Thus, one can conclude that at high temperature, i.e., 550 °C, the diffusion limitations of iso-butane within the MFI framework with flexibility[64] are still more severe than that in BEA framework. This conclusion agrees with the results of the FFMD simulations.

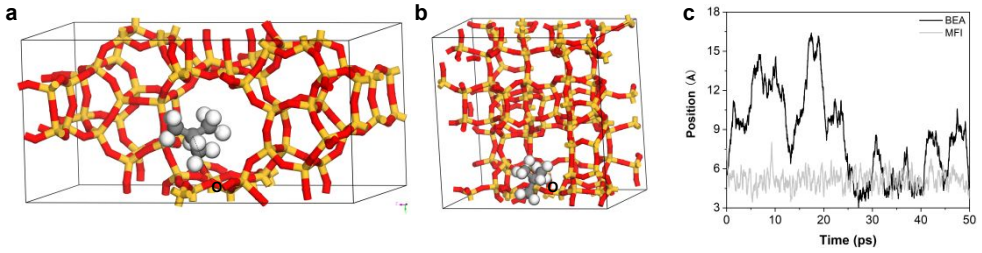

Figure 7 The definition of relative position between iso-butane and selected oxygen atom in (a) BEA and (b) MFI frameworks. (c) The evolution of relative displacement of iso-butane within BEA and MFI frameworks at 550 ˚C obtained by AIMD simulations. Black circles in (a) and (b) stand for oxygen atoms.

3.7 Consequences of Diffusion Constrains for Product Selectivity

To understand if and how diffusion constrains affect selectivity to gas-phase products and coke in the iBDH reaction over ZnO-zeolite based catalysts, we analyzed selectivity-conversion relationships obtained from steady-state tests carried out at different contact time. For comparative purposes, the corresponding data for the PDH reaction were also analyzed, although no mass transport limitations are expected for this reaction under our reaction conditions. Regardless of the type of zeolite and the feed alkane, the selectivity to the desired olefins decreases with increasing alkane conversion, while the selectivity to

cracking products and coke follow an opposite trend (Figure 8a-f). The selectivity to propene or isobutene extrapolated to zero conversion of propane or isobutane starts is close to 1, while the selectivity to coke and cracking products is close to 0. This is a fingerprint for the existence of the only one direct pathway of alkane conversion, i.e., the dehydrogenation to the corresponding olefins. They undergo further transformations to secondary products, i.e., cracking products and coke (Figure 8g).

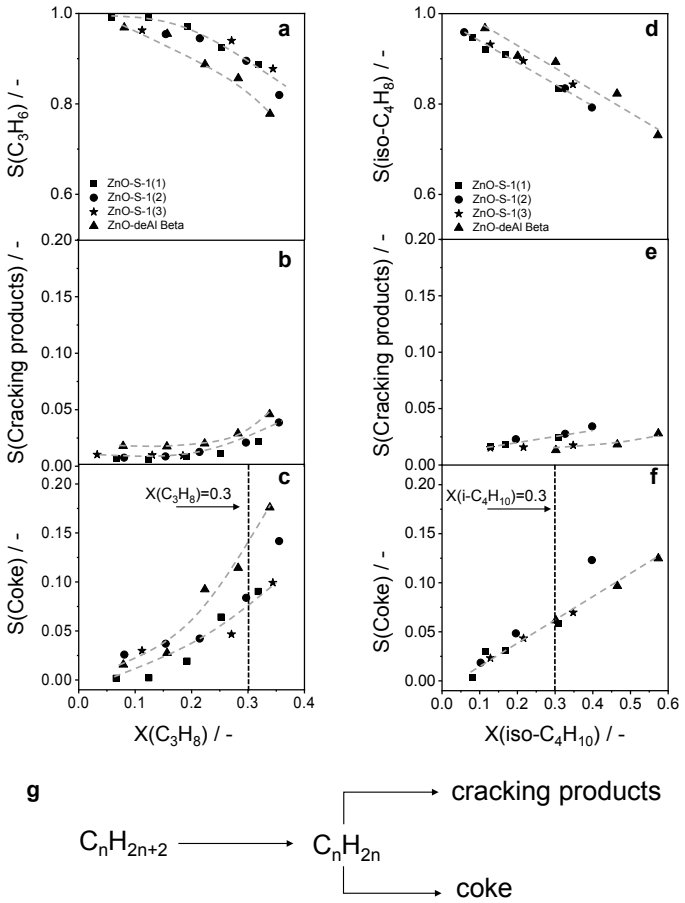

Figure 8 Dependence of selectivity to propene, isobutene, coke and cracking products on conversion of propane (a)-(c) or isobutane (d)-(f) over ZnO-zeolite catalysts. (g). The proposed pathways of products formation. Reaction conditions: 550 ℃, C_nH_{2n+2}:N_2=2:3, n=3 or 4

In the PDH reaction (no mass transport limitations), the ZnO-S-1(i) catalysts show higher propene selectivity in the whole range of degrees of propane conversion in comparison

with the ZnO-deAl Beta catalyst. Consequently, the latter material is characterized by higher selectivity to coke (Figure 8c). This can be caused by the residual acidic Al^{3+} cations in the support as proved by NH_3-TPD tests (Figure S13) or by the nature of ZnO_x species in deAl Beta, which shows higher intrinsic selectivity to coke in comparison with ZnO_x species in S-1. However, when the same catalysts were used in the iBDH reaction, the ZnO-deAl Beta catalyst showed higher isobutene selectivity than the ZnO-S-1(i) catalysts. Thus, the kind of ZnO_x can be excluded as the reason for the differ selectivity over these materials. To explain the changes in the selectivity order between the ZnO-deAl Beta and ZnO-S-1(i) catalysts in PDH and iBDH, the diffusivity of isobutene inside the MFI and BEA frameworks was also simulated (Figure S14). The diffusion of this olefin inside the BEA framework is more than 30 times faster than that inside the MFI framework (Table S5). Thus, secondary reactions isobutene over ZnO-deAl Beta were inhibited to some extent in comparison with ZnO-S-1(i) catalysts. As all these catalysts also differ in the selectivity to cracking products but not to coke in iBDH, we suggest that cracking reactions of isobutene are favored when the effectiveness factor is low.

4 CONCLUSIONS

The morphology of ZrO_2, S-1 and Beta zeolite supports was established to (i) determine the kind of catalytically active ZnO_x sites formed from a physical mixture of ZnO and support under propane/isobutane dehydrogenation conditions and (ii) to control olefin selectivity through limited diffusion of the desired product. Regardless of the zeolite

morphology, catalytically active ZnO_x species are formed inside the pores. Binuclear ZnO_x species and 3-dimentional multinuclear ZnO_x clusters were in situ formed on the internal surface of silicalite-1 and deAl Beta zeolite, respectively. The external surface of ZrO_2 is populated by binuclear ZnO_x species differing from those in silicalite-1.

Both experimental results and theoretical force field molecular dynamics (FFMD) simulations prove that propane molecules do not have any significant diffusion constrains within the S-1 and deAl-Beta zeolites ($\eta>0.8$). Contrarily, the diffusion of isobutane and isobutene inside the S-1 framework is hindered. In addition to low utilization efficiency ($\eta<0.45$) of the active sites, the internal diffusion limitations cause loss in the selectivity to isobutene due to its consecutive conversion into C_1-C_3 hydrocarbons.

Under conditions free of any diffusion limitations, ZnO_x clusters reveal higher Zn-related activity than binuclear ZnO_x species. The theoretical calculations revealed that breaking of the C-H bonds in iso-C_4H_{10} requires higher energies in comparison with C_3H_8 molecule due to the steric effect of the iso-C_4H_9 intermediate, while lower energy span was needed for the whole iso-C_4H_{10} dehydrogenation processes.

ASSOCIATED CONTENT

Supporting Information. This material is available free of charge via the Internet at http://pubs.acs.org. The structures of MFI and BEA zeolite, the SEM images of different supports, the EXAFS fits, the DRIFTs spectra of different supports, the temperature

programmed release of water over different supports, the Arrhenius plots in PDH and iBDH reactions over different supports, the catalytic performance of different catalysts, the ZnO_x/S-1 model for DFT calculations, the potential energy surface of isobutane dehydrogenation, intermediates in iBDH reaction over ZnO_x/S-1 catalyst, NH_3-TPD profiles of supports, the diffusion data and the comparison of ZnO-based catalysts and the state-of-the-art catalysts in the PDH and iBDH reactions are included.

AUTHOR INFORMATION

Corresponding Author

Evgenii V. Kontratenko - Leibniz-Institut für Katalyse e. V., Albert-Einstein-Strasse 29A, 18059 Rostock, Germany, ORCID: 0000-0003-0431-6937

E-Mail: evgenii.kondratenko@catalysis.de (EVK)

Author Contributions

E.V.K. initiated and led the whole project. D.Z, M.G and X.T contributed equally to this work. D.Z. prepared all the catalysts, carried out catalytic tests and characterization measurements. M.G and M.Y performed force field molecular dynamics simulation and analyzed the results, as well as wrote the corresponding part in the manuscript. X.T and H.J performed DFT calculation and wrote the corresponding part in the manuscript. D.E.D. and J.D.G. performed XAS experiments and, with D.Z., analyzed the results. All the authors discussed the results and improved the manuscript.

Notes

The authors declare no competing financial interest.

ACKNOWLEDGEMENT

Financial support by Deutsche Forschungsgemeinschaft (KO 2261/8-1), the National Natural Science Foundation of China (Grant Nos 21961132026, 21878331 and 91645108), Science Foundation of China University of Petroleum, Beijing (C201604) and the State of Mecklenburg-Vorpommern are gratefully acknowledged. The authors also thank Reinhard Eckelt for BET measurements. We acknowledge DESY (Hamburg, Germany), a member of the Helmholtz Association HGF, for the prevision of experimental facilities. Parts of this research were carried out at PETRA III and we would like to thank Dr. Edmund Welter for assistance in using beamline P65.

REFERENCES

1.Liu, Z.; Zhou, J.; Tang, X.; Liu, F.; Yuan, J.; Li, G.; Huang, L.; Krishna, R.; Huang, K.; Zheng, A., Dependence of zeolite topology on alkane diffusion inside diverse channels *AIChE Journal* **2020**, 66 (8), e16269.

2.Chassaing, S.; Alix, A.; Olmos, A.; Keller, M.; Sommer, J.; Pale, P., Metal-doped Zeolites as Green Catalysts for Organic Synthesis *Zeitschrift für Naturforschung B* **2010**, 65, 783-790.

3.Dai, X.; Wang, X.; Rabeah, J.; Kreyenschulte, C.; Bruckner, A.; Shi, F., Supported Cu(II) Single-Ion Catalyst for Total Carbon Utilization of C2 and C3 Biomass-Based Platform Molecules in the N-Formylation

of Amines *Eur. J. Chem.* **2021**, 27 (68), 16889-16895.

4.Liu, G.; Liu, J.; He, N.; Miao, C.; Wang, J.; Xin, Q.; Guo, H., Silicalite-1 zeolite acidification by zinc modification and its catalytic properties for isobutane conversion *RSC Advances* **2018**, 8 (33), 18663-18671.

5.Yang, Q.; Li, Y.; Chen, Z.; Hu, L.; Li, Z.; Wang, Y.; Zhao, Z.; Xu, C.; Jiang, G., Core-shell structured HZSM-5@mesoSiO$_2$ catalysts with tunable shell thickness for efficient n-butane catalytic cracking *AIChE J* **2021**, 67 (4), e17130.

6.Hu, S.; Liu, J.; Ye, G.; Zhou, X.; Coppens, M. O.; Yuan, W., Effect of External Surface Diffusion Barriers on Platinum/Beta-Catalyzed Isomerization of n-Pentane *Angew Chem Int Ed Engl* **2021**, 60 (26), 14394-14398.

7.Otroshchenko, T.; Jiang, G.; Kondratenko, V. A.; Rodemerck, U.; Kondratenko, E. V., Current status and perspectives in oxidative, non-oxidative and CO_2-mediated dehydrogenation of propane and isobutane over metal oxide catalysts *Chem Soc Rev* **2021**, 50 (1), 473-527.

8.Li, C.; Wang, G., Dehydrogenation of light alkanes to mono-olefins *Chem Soc Rev* **2021**, 50 (7), 4359-4381.

9.Chen, S.; Chang, X.; Sun, G.; Zhang, T.; Xu, Y.; Wang, Y.; Pei, C.; Gong, J., Propane dehydrogenation: catalyst development, new chemistry, and emerging technologies *Chem Soc Rev* **2021**, 50 (5), 3315-3354.

10.Nakaya, Y.; Xing, F.; Ham, H.; Shimizu, K. I.; Furukawa, S., Doubly Decorated Platinum-Gallium Intermetallics as Stable Catalysts for Propane Dehydrogenation *Angew Chem Int Ed Engl* **2021**, 60 (36), 19715-19719.

11.Chen, X.; Peng, M.; Cai, X.; Chen, Y.; Jia, Z.; Deng, Y.; Mei, B.; Jiang, Z.; Xiao, D.; Wen, X.; Wang, N.; Liu, H.; Ma, D., Regulating coordination number in atomically dispersed Pt species on defect-rich

graphene for n-butane dehydrogenation reaction *Nat Commun* **2021**, 12 (1), 2664.

12.Ali Hussain Motagamwala, R. A., James Wortman,; Valentina Omoze Igenegbai, S. L., Stable and selective catalysts for propane dehudrogenation operating at thermodynamic limit *Science* **2021**, 373, 217-222.

13.Bert M. Weckhuysen, R. A. S., Alkane dehydrogeantion over supported chromium oxide catalysts. *Catal. Today* **1999**, 51, 223-232.

14.Masoudian, S. K.; Sadighi, S.; Abbasi, A.; Salehirad, F.; Fazlollahi, A., Regeneration of a Commercial Catalyst for the Dehydrogenation of Isobutane to Isobutene *Chem. Eng. Technol.* **2013**, 36 (9), 1593-1598.

15.Rodemerck, U.; Stoyanova, M.; Kondratenko, E. V.; Linke, D., Influence of the kind of VO_x structures in VO_x/MCM-41 on activity, selectivity and stability in dehydrogenation of propane and isobutane *J. Catal.* **2017**, 352, 256-263.

16.Zhao, Z. J.; Wu, T.; Xiong, C.; Sun, G.; Mu, R.; Zeng, L.; Gong, J., Hydroxyl-Mediated Non-oxidative Propane Dehydrogenation over VO_x/gamma-Al_2O_3 Catalysts with Improved Stability *Angew Chem Int Ed Engl* **2018**, 57 (23), 6791-6795.

17.Sattler, J. J.; Gonzalez-Jimenez, I. D.; Luo, L.; Stears, B. A.; Malek, A.; Barton, D. G.; Kilos, B. A.; Kaminsky, M. P.; Verhoeven, T. W.; Koers, E. J.; Baldus, M.; Weckhuysen, B. M., Platinum-promoted Ga/Al_2O_3 as highly active, selective, and stable catalyst for the dehydrogenation of propane *Angew Chem Int Ed Engl* **2014**, 53 (35), 9251-6.

18.Castro-Fernández, P.; Mance, D.; Liu, C.; Moroz, I. B.; Abdala, P. M.; Pidko, E. A.; Copéret, C.; Fedorov, A.; Müller, C. R., Propane Dehydrogenation on Ga_2O_3-Based Catalysts: Contrasting Performance with Coordination Environment and Acidity of Surface Sites *ACS Catal.* **2021**, 11 (2), 907-924.

19.Chen, C.; Zhang, S.; Wang, Z.; Yuan, Z.-Y., Ultrasmall Co confined in the silanols of dealuminated beta zeolite: A highly active and selective catalyst for direct dehydrogenation of propane to propylene *J. Catal.* **2020**, 383, 77-87.

20.Yang, Z.; Li, H.; Zhou, H.; Wang, L.; Wang, L.; Zhu, Q.; Xiao, J.; Meng, X.; Chen, J.; Xiao, F. S., Coking-Resistant Iron Catalyst in Ethane Dehydrogenation Achieved through Siliceous Zeolite Modulation *J. Am. Chem. Soc.* **2020**, 142 (38), 16429-16436.

21.Hu, B.; Schweitzer, N. M.; Zhang, G.; Kraft, S. J.; Childers, D. J.; Lanci, M. P.; Miller, J. T.; Hock, A. S., Isolated Fe^{II} on Silica As a Selective Propane Dehydrogenation Catalyst *ACS Catal.* **2015**, 5 (6), 3494-3503.

22.Otroshchenko, T.; Sokolov, S.; Stoyanova, M.; Kondratenko, V. A.; Rodemerck, U.; Linke, D.; Kondratenko, E. V., ZrO_2-Based Alternatives to Conventional Propane Dehydrogenation Catalysts: Active Sites, Design, and Performance *Angew Chem Int Ed Engl* **2015**, 54 (52), 15880-3.

23.Zhang, Y.; Zhao, Y.; Otroshchenko, T.; Lund, H.; Pohl, M. M.; Rodemerck, U.; Linke, D.; Jiao, H.; Jiang, G.; Kondratenko, E. V., Control of coordinatively unsaturated Zr sites in ZrO_2 for efficient C-H bond activation *Nat Commun* **2018**, 9 (1), 3794.

24.Schweitzer, N. M.; Hu, B.; Das, U.; Kim, H.; Greeley, J.; Curtiss, L. A.; Stair, P. C.; Miller, J. T.; Hock, A. S., Propylene Hydrogenation and Propane Dehydrogenation by a Single-Site Zn^{2+} on Silica Catalyst *ACS Catal.* **2014**, 4 (4), 1091-1098.

25.Liu, G.; Zeng, L.; Zhao, Z.-J.; Tian, H.; Wu, T.; Gong, J., Platinum-Modified ZnO/Al_2O_3 for Propane Dehydrogenation: Minimized Platinum Usage and Improved Catalytic Stability *ACS Catal.* **2016**, 6 (4), 2158-2162.

26.Han, S.; Zhao, D.; Lund, H.; Rockstroh, N.; Bartling, S.; Doronkin, D. E.; Grunwaldt, J.-D.; Gao, M.;

Jiang, G.; Kondratenko, E. V., TiO_2-Supported catalysts with ZnO and ZrO_2 for non-oxidative dehydrogenation of propane: mechanistic analysis and application potential *Catal. Sci. Tech.* **2020**, 10 (20), 7046-7055.

27.Han, S.; Zhao, D.; Otroshchenko, T.; Lund, H.; Bentrup, U.; Kondratenko, V. A.; Rockstroh, N.; Bartling, S.; Doronkin, D. E.; Grunwaldt, J.-D.; Rodemerck, U.; Linke, D.; Gao, M.; Jiang, G.; Kondratenko, E. V., Elucidating the Nature of Active Sites and Fundamentals for their Creation in Zn-Containing ZrO_2–Based Catalysts for Nonoxidative Propane Dehydrogenation *ACS Catal.* **2020**, 10 (15), 8933-8949.

28.Almutairi, S. M. T.; Mezari, B.; Magusin, P. C. M. M.; Pidko, E. A.; Hensen, E. J. M., Structure and Reactivity of Zn-Modified ZSM-5 Zeolites: The Importance of Clustered Cationic Zn Complexes *ACS Catal.* **2011**, 2 (1), 71-83.

29.Gong, T.; Qin, L.; Lu, J.; Feng, H., ZnO modified ZSM-5 and Y zeolites fabricated by atomic layer deposition for propane conversion *Phys Chem Chem Phys* **2016**, 18 (1), 601-14.

30.Chen, C.; Hu, Z.; Ren, J.; Zhang, S.; Wang, Z.; Yuan, Z.-Y., ZnO Nanoclusters Supported on Dealuminated Zeolite β as a Novel Catalyst for Direct Dehydrogenation of Propane to Propylene *ChemCatChem* **2019**, 11 (2), 868-877.

31.Zhao, D.; Guo, K.; Han, S.; Doronkin, D. E.; Lund, H.; Li, J.; Grunwaldt, J.-D.; Zhao, Z.; Xu, C.; Jiang, G.; Kondratenko, E. V., Controlling Reaction-Induced Loss of Active Sites in ZnO_x/Silicalite-1 for Durable Nonoxidative Propane Dehydrogenation *ACS Catal.* **2022**, 12 (8), 4608-4617.

32.Zhao, D.; Tian, X.; Doronkin, D. E.; Han, S.; Kondratenko, V. A.; Grunwaldt, J.-D.; Perechodjuk, A.; Vuong, T. H.; Rabeah, J.; Eckelt, R.; Rodemerck, U.; Linke, D.; Jiang, G.; Jiao, H.; Kondratenko, E. V., In situ formation of ZnO_x species for efficient propane dehydrogenation *Nature* **2021**, 599 (7884), 234-238.

33.Xie, L.; Wang, R.; Chai, Y.; Weng, X.; Guan, N.; Li, L., Propane dehydrogenation catalyzed by in-situ partially reduced zinc cations confined in zeolites *J. Energy Chem.* **2021**, 63, 262-269.

34.Liu, J.; Liu, Y.; Liu, H.; Fu, Y.; Chen, Z.; Zhu, W., Silicalite-1 Supported ZnO as an Efficient Catalyst for Direct Propane Dehydrogenation *ChemCatChem* **2021**, 13, 4780-4786.

35.Zhao, D.; Li, Y.; Han, S.; Zhang, Y.; Jiang, G.; Wang, Y.; Guo, K.; Zhao, Z.; Xu, C.; Li, R.; Yu, C.; Zhang, J.; Ge, B.; Kondratenko, E. V., ZnO Nanoparticles Encapsulated in Nitrogen-Doped Carbon Material and Silicalite-1 Composites for Efficient Propane Dehydrogenation *iScience* **2019**, 13, 269-276.

36.Ravel, B.; Newville, M., ATHENA, ARTEMIS, HEPHAESTUS: data analysis for X-ray absorption spectroscopy using IFEFFIT *J Synchrotron Radiat* **2005**, 12 (Pt 4), 537-41.

37.Qi, L.; Babucci, M.; Zhang, Y.; Lund, A.; Liu, L.; Li, J.; Chen, Y.; Hoffman, A. S.; Bare, S. R.; Han, Y.; Gates, B. C.; Bell, A. T., Propane Dehydrogenation Catalyzed by Isolated Pt Atoms in identical with SiOZn-OH Nests in Dealuminated Zeolite Beta *J Am Chem Soc* **2021**, 143 (50), 21364-21378.

38.Beerdsen, E.; Smit, B.; Dubbeldam, D., Molecular Simulation of Loading Dependent Slow Diffusion in Confined Systems *Phys. Rev. Lett.* **2004**, 93 (24), 248301.

39.Skoulidas, A. I.; Sholl, D. S., Molecular Dynamics Simulations of Self-Diffusivities, Corrected Diffusivities, and Transport Diffusivities of Light Gases in Four Silica Zeolites To Assess Influences of Pore Shape and Connectivity *J. Phys. Chem. A* **2003**, 107 (47), 10132-10141.

40.Liu, Z.; Zhou, J.; Tang, X.; Liu, F.; Yuan, J.; Li, G.; Huang, L.; Krishna, R.; Huang, K.; Zheng, A., Dependence of Zeolite Topology on Alkane Diffusion inside Nano-Channels *AIChE J.* **2020**, 66 (8), e16269.

41.Cnudde, P.; Demuynck, R.; Vandenbrande, S.; Waroquier, M.; Sastre, G.; Speybroeck, V. V., Light Olefin Diffusion during the MTO Process on H-SAPO-34: A Complex Interplay of Molecular Factors *J. Am. Chem.*

Soc. **2020**, 142 (13), 6007-6017.

42.Xiong, H.; Liu, Z.; Chen, X.; Wang, H.; Qian, W.; Zhang, C.; Zheng, A.; Wei, F., In situ imaging of the sorption-induced subcell topological flexibility of a rigid zeolite framework *Science* **2022**, 376 (6592), 491-496.

43.Hutter, J.; Iannuzzi, M.; Schiffmann, F.; VandeVondele, J., cp2k: atomistic simulations of condensed matter systems *WIREs Computational Molecular Science* **2014**, 4 (1), 15-25.

44.Lippert, G.; Hutter, J.; Parrinello, M., The Gaussian and augmented-plane-wave density functional method for ab initio molecular dynamics simulations *Theor. Chem. Acc.* **1999**, 103 (2), 124-140.

45.Yang, K.; Zheng, J.; Zhao, Y.; Truhlar, D. G., Tests of the RPBE, revPBE, τ-HCTHhyb, ωB97X-D, and MOHLYP density functional approximations and 29 others against representative databases for diverse bond energies and barrier heights in catalysis *Chem. Phys.* **2010**, 132 (16), 164117.

46.Goedecker, S.; Teter, M.; Hutter, J., Separable dual-space Gaussian pseudopotentials *Physical Review B* **1996**, 54 (3), 1703-1710.

47.Grimme, S.; Antony, J.; Ehrlich, S.; Krieg, H., A consistent and accurate ab initio parametrization of density functional dispersion correction (DFT-D) for the 94 elements H-Pu *Chem. Phys.* **2010**, 132 (15), 154104.

48.Grimme, S.; Ehrlich, S.; Goerigk, L., Effect of the damping function in dispersion corrected density functional theory *J. Comput. Chem.* **2011**, 32 (7), 1456-1465.

49.Nosé, S., A unified formulation of the constant temperature molecular dynamics methods *Chem. Phys.* **1984**, 81 (1), 511-519.

50.Hoover, W. G., Canonical dynamics: Equilibrium phase-space distributions *Phys. Rev. A* **1985**, 31 (3),

1695-1697.

51.Martyna, G. J.; Klein, M. L.; Tuckerman, M., Nosé–Hoover chains: The canonical ensemble via continuous dynamics *Chem. Phys.* **1992**, 97 (4), 2635-2643.

52.Martyna, G. J.; Tobias, D. J.; Klein, M. L., Constant pressure molecular dynamics algorithms *Chem. Phys.* **1994**, 101 (5), 4177-4189.

53.G. Kresse; Furthmueller, J., Efficiency of ab-initio total energy calculation for metals and semiconductors using a plane-wave basis set *Computational Materials Science* **1996**, 6, 15-50.

54.Kresse, G.; Furthmueller, J., Efficient iterative schemes for ab initio total energy calculations using a plane-wave basis set *Physical Review B* **1996**, 54, 11169-11186.

55.John P. Perdew; Kieron Burke; Ernzerhof, M., Generalized gradient approximation made simple *Phys. Rev. Lett* **1996**, 77, 3865-3868.

56.John P. Perdew; Kieron Burke; Ernzerhof, M., Generalized Gradient Approximation Made Simple *Phys. Rev. Lett* **1997**, 78, 1396.

57.Graeme Henkelman; Blas P. Uberuaga; Jónsson, H., A climbing image nudged elastic band method for finding saddle points and minimum energy paths *J. Chem. Phys.* **2000**, 113 (22), 9901-9904.

58.Han, J.; Liu, Z.; Li, H.; Zhong, J.; Zhang, W.; Huang, J.; Zheng, A.; Wei, Y.; Liu, Z., Simultaneous Evaluation of Reaction and Diffusion over Molecular Sieves for Shape-Selective Catalysis *ACS Catal.* **2020**, 10 (15), 8727-8735.

59.Gao, M.; Li, H.; Liu, W.; Xu, Z.; Peng, S.; Yang, M.; Ye, M.; Liu, Z., Imaging spatiotemporal evolution of molecules and active sites in zeolite catalyst during methanol-to-olefins reaction *Nat. Commun.* **2020**, 11 (1), 3641-3652.

60.Song, L.; Rees, L. V. C., Frequency response diffusion of propane in silicalite-1 *Microporous Mater.* **1996**, 6 (5), 363-374.

61.Zhu, W.; Malekian, A.; Eić, M.; Kapteijn, F.; Moulijn, J. A., Concentration-dependent diffusion of isobutane in silicalite-1 studied with the ZLC technique *Chem. Eng. Sci.* **2004**, 59 (18), 3827-3835.

62.Dubbeldam, D.; Snurr, R. Q., Recent developments in the molecular modeling of diffusion in nanoporous materials *Mol. Simul.* **2007**, 33 (4-5), 305-325.

63.Haldoupis, E.; Nair, S.; Sholl, D. S., Pore size analysis of >250,000 hypothetical zeolites *Phys Chem Chem Phys* **2011**, 13 (11), 5053-60.

64.Caro-Ortiz, S.; Zuidema, E.; Rigutto, M.; Dubbeldam, D.; Vlugt, T. J. H., Effects of Framework Flexibility on the Adsorption and Diffusion of Aromatics in MFI-Type Zeolites *J. Phys. Chem. C* **2020**, 124 (44), 24488-24499.

TOC